Cylindrical Coplanar Waveguide Transition Circuit for Microwave Connections on Curved Surfaces

1st Benyamin Harkinezhad
KU Leuven
Leuven, Belgium
https://orcid.org/0000-0002-1700-3596

2nd Tomislav Markovic
University of Zagreb
Zagreb, Croatia
https://orcid.org/0000-0002-9645-5565

3rd Robin Evans
University of Melbourne
Melbourne, Australia
https://orcid.org/0000-0002-7988-3189

4th Kamran Ghorbani
RMIT University
Melbourne, Australia
https://orcid.org/0000-0001-8767-0207

5th Efstratios Skafidas
University of Melbourne
Melbourne, Australia
https://orcid.org/0000-0003-4263-9972

6th Dominique Schreurs
KU Leuven
Leuven, Belgium
https://orcid.org/0000-0002-4018-7936

***Abstract*—External connections are critical in microwave circuits, and designing impedance-matched coaxial transitions is a key challenge. While planar circuit transitions are well-studied, limited attention has been given to transitions for curved surfaces, such as vials and test tubes commonly encountered in chemical and biomedical laboratories. With the growing demand for accurate in-situ measurements in these applications, addressing this gap has become increasingly important. This work introduces a novel transition from coaxial to coplanar waveguide (CPW) mode on a cylindrical surface, specifically designed for use with curved containers like vials. The proposed transition achieves a minimum return loss of 12 dB within the DC–10 GHz band and maintains an insertion loss below 1 dB up to 6 GHz. Fabricated on a semi-flexible substrate, the design is well-suited for biomedical sensing and in-situ measurements of cylindrical samples.**

***Index Terms*—biomedical sensing, cylindrical coplanar waveguide (CCPW), flexible microwave interconnects, in-situ material characterization, non-planar microwave circuits**

I. Introduction

Microwave connectors are primarily designed for flat printed circuit board (PCB) technology, making them unsuitable for non-planar geometries. However, in many practical applications, particularly in chemical and biological laboratories, sensors perform better when their geometry conforms to that of the sample [1], [2]. Similarly, in biomedical applications, wearable microwave sensors are increasingly used for on-skin measurements, highlighting the need for microwave interconnects that can adapt to curved surfaces [3].

Although flexible microwave sensors have been developed to match the shape of curved samples [4], [5], integrating effective connections remains a challenge. Flexible interconnects are essential to fully exploit sensor flexibility, thereby enhancing performance. Yet, research on flexible microwave interconnects has been limited. Existing solutions often integrate rigid connector interfaces within flexible systems or position the connectors away from the sensing region, leading to suboptimal performance [6], [7]. While some textile-based microwave antennas incorporate flexible connectors, they often suffer from bandwidth limitations [8], [9].

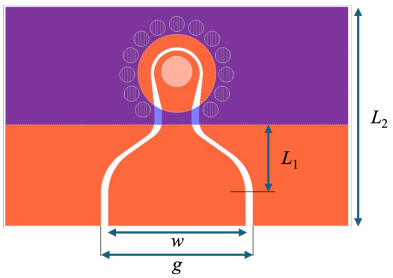

Fig. 1. Design of the coaxial-to-CCPW transition circuit. The red layer is the top conductor, the blue layer is the bottom ground plane, and vias (hashed circles) provide grounding. The white hole allows the SMA connector's center pin to pass through and solder onto the CPW signal trace on the top layer. Key dimensions: $w = 7.2$ mm, $g = 8$ mm, $L_1 = 3.4$ mm, $L_2 = 11.5$ mm.

This work presents a novel transition circuit designed on a semi-flexible substrate to enable microwave interconnects for cylindrical samples commonly found in laboratory settings. The proposed design has been tested on a 16 mm diameter vial, a commonly used size in laboratory settings, and is expected to accommodate other cylindrical samples within a similar range.

II. Design and Fabrication

A. Design

The transition design is schematically presented in Fig. 1. The designed circuit provides a transition between a conductor-backed coplanar waveguide (CBCPW) (top part) and a conventional coplanar waveguide (CPW) (bottom part). The design is compatible with flange-mount SMA connectors. A circular section of the bottom layer ground plane (blue) is removed to accommodate the SMA connector's dielectric, enabling the connector to be mounted from the backside of the circuit. The center conductor of the SMA connector protrudes through the transition substrate and is joined to the CPW signal trace on the top layer (red).

To suppress parallel-plate waveguide mode and other undesired effects in the CBCPW, the top and bottom layer

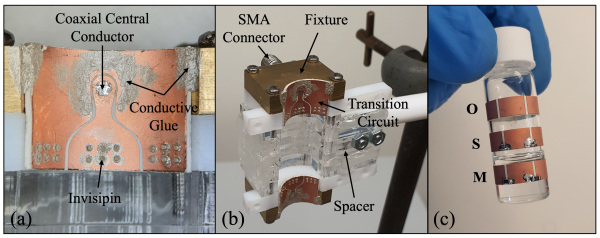

Fig. 2. Fabricated fixture-transition circuit assembly. (a) Close-up of the transition circuit installed in the fixture with conductive glue ensuring grounding to the brass base. (b) Two-port measurement setup with fixture-transition circuit assemblies connected via a spacer to ensure proper alignment and spacing. (c) Open, short, and 50 Ω load de-embedding standards, labeled as 'O', 'S', and 'M', respectively, wrapped around a glass vial.

ground planes are via-stitched. The CBCPW is then tapered to transition smoothly to the CPW. To enable connections with Cylindrical CPW (CCPW) circuits, i.e., CPWs on cylindrical surfaces, connectors known as Invisipins®, which become conductive upon compression, are attached to the ends of the CPW line (Fig. 2a). These connectors are chosen for their low compression force and compact size, making them suitable for surfaces with high curvature.

B. Fabrication

In this work, the transition circuit is fabricated on a 0.76 mm thick Rogers RO3003 substrate ($\epsilon_r = 3.0$, $tan\delta = 0.001$). For testing purposes, also a custom fixture was developed to accommodate the transition circuit. The fixture features a brass part on the top with mounting screw holes and a 4.1 mm diameter hole to accommodate the 12.7 mm protruding dielectric and center conductor of a flange-mount SMA connector. The opposite side includes a circular cavity with 8.9 mm radius, designed to hold the transition circuit. This part was made from brass to provide grounding for the SMA connector and establish continuity between its ground and that of the transition circuit. The remaining parts of the fixture are made of PTFE. The transition circuit is affixed to the brass section using conductive adhesive to ensure electrical and mechanical connections. The image of the transition circuit mounted on the fixture is given in Fig. 2.

For de-embedding purposes, open, short, and 50 Ω load standards were designed using a CCPW on a 0.05 mm thick Rogers Ultralam 3850HT substrate ($\epsilon_r = 2.9$, $tan\delta = 0.002$) wrapped around a glass vial with 1.2 mm wall thickness and 16 mm outer diameter. The 50 Ω load standard was fabricated by soldering two 100 Ω, 0805 surface-mount resistors between the CPW signal trace and ground planes on a 5 mm long CCPW section. The short and open standards were fabricated using the same CCPW structure (Fig. 2c).

III. Simulations and Measurements

A. Simulations

The performance of the designed transition circuit, in combination with the fixture, was characterized using 3D finite element method (FEM) simulations. The simulated configuration included the fixture and transition circuit integrated with

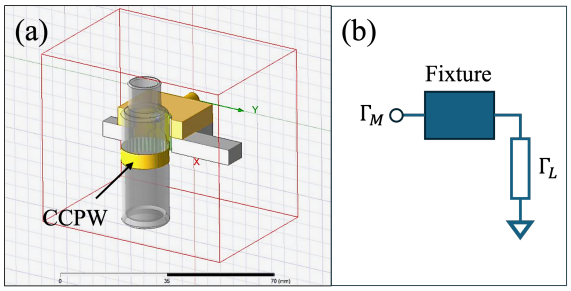

Fig. 3. Simulation and de-embedding setup for the designed fixture and transition circuit. (a) The image shows the FEM simulation window with a vial inserted into the fixture. The vial features a 5 mm CCPW wrapped around it. (b) Schematic diagram of the de-embedding configuration, showing the fixture connected to a load.

a 5 mm long CCPW wrapped around a vial with a diameter of 16 mm, as shown in Fig. 3. This setup allowed for the determination of the *S*-parameters, including the effects of the transition between the Invisipins and the CCPW on the vial.

To excite the structure, modal wave ports were assigned to the SMA connector at the back of the fixture and to the lower end of the CCPW on the vial. The simulation mesh was adaptively refined, with a maximum tolerance of 0.01 in the *S*-parameters at the maximum simulation frequency. The frequency sweep was performed adaptively over the range of 10 MHz to 10 GHz.

B. De-embedding

An Open-Short-Match (OSM) de-embedding scheme is used to extract the *S*-parameters of the combined fixture and transition circuit. The de-embedding was applied to shift the reference plane to 5 mm from the edge of the CCPW on the glass vial. Since the fixture is reciprocal, only three unknowns need to be determined: S_{11}, S_{22}, and $S_{12}S_{21}$. A schematic of the fixture with a load attached at Port 2 is shown in Fig. 3b.

The *S*-parameters of this configuration are given by:

$$\Gamma_M = \frac{S_{11} - |\mathbf{S}|\Gamma_L}{1 - \Gamma_L S_{22}} \tag{1}$$

where Γ_M represents the measured S_{11} parameter (distinct from the S_{11} of the fixture). By performing three measurements using the previously described calibration standards, a system of three equations with three unknowns (S_{11}, S_{22}, and $S_{12}S_{21}$) is obtained, allowing for their unique determination.

Further de-embedding of the 5 mm CCPW line was deemed unnecessary, as the reference plane was deliberately placed away from the Invisipin-to-CCPW transition to enhance the accuracy of the de-embedded *S*-parameters.

C. Measurement Results

Fig. 4 shows the de-embedded *S*-parameters of the fabricated fixture. Observing S_{11} in Fig. 4(a), the return loss exhibits adequate performance, as S_{11} remains below -12 dB within the band of interest. The differences between the measurements and simulations are likely due to fabrication

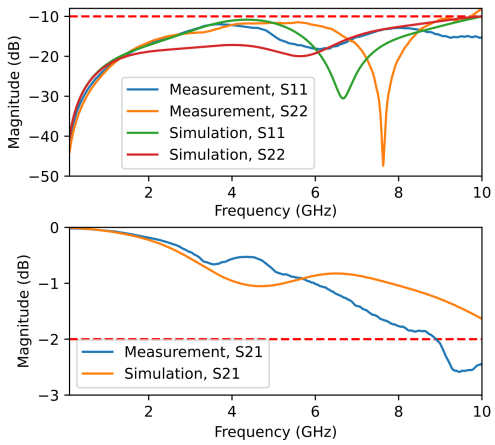

Fig. 4. De-embedded S-parameters of the fabricated fixture. Measured S-parameters were obtained using reference measurements with calibration standards fabricated on a CCPW wrapped around the glass vial.

tolerances and the omission of the return and insertion losses of the Invisipins in the simulations. However, examining S_{22}, the fixture performs optimally below 9 GHz, as reflections exceed the acceptable limit beyond this frequency. At higher frequencies, the accuracy of the de-embedding process becomes questionable due to the non-ideal behavior of the calibration standards.

The transmission losses, shown in Fig. 4b, remain below 1 dB up to 6 GHz. The S_{21} parameter drops below -2 dB at 9 GHz. The primary source of losses occurs at the transition between the coaxial mode and the CBCPW circuit. This is largely due to the flat-ended dielectric of the SMA connector, which does not conform to the curvature of the transition circuit, creating an air gap at the interface. Increasing the bending radius to reduce the curvature of the circuit can mitigate this issue. A more effective solution, however, would involve using flange-mount connectors with air as the dielectric, such as 2.92 mm connectors.

Additionally, the current design mounts the SMA connector from the bottom layer of the transition circuit, resulting in the substrate to act as the dielectric for the connector over a distance equal to the substrate thickness. While reducing the substrate thickness could minimize this effect, it cannot be completely avoided due to the geometry of the design.

Further improvements could be achieved by eliminating the transition from CBCPW to CPW and instead using CBCPW throughout the circuit. This would reduce the CPW dimensions at the lower end of the transition, simplifying connections and reducing the impact of curvature on performance.

A fixture integrating an early version of this transition circuit was utilized for two-port measurements on a CCPW wrapped around a plastic test tube, where materials such as NaCl and KCl were successfully characterized [10]. This application highlights the fixture's ability for accurate in-situ material characterization, further validating its suitability for biomedical and chemical applications.

IV. Conclusion

This work presents a novel transition circuit for enabling microwave interconnects on curved surfaces, addressing a key challenge in non-planar microwave applications. The proposed semi-flexible design is compatible with cylindrical holders commonly used in chemical and biomedical contexts.

Measurements confirm the circuit performs well up to 6 GHz, achieving a return loss better than 12 dB within the DC–10 GHz band and an insertion loss below 1 dB up to 6 GHz. Losses primarily arise at the coaxial-to-CBCPW transition, due to air gaps caused by curvature mismatch with the SMA connector's dielectric. Increasing the bending radius or using connectors with air as a dielectric could mitigate these losses. Eliminating the CBCPW-to-CPW transition may further enhance performance by simplifying connections and reducing the impact of curvature.

This work establishes a foundation for future improvements in microwave interconnects for curved surfaces. Future efforts will explore the effect of varying bending radii on the circuit's performance and focus on optimizing the design to improve performance within and beyond the current frequency range, along with developing fully flexible solutions for applications in wearable electronics and biomedical sensing.

Acknowledgment

This research was supported by KU Leuven funding for the project C24E/20/035 MESMERIC, FWO funding for the project G0E3921N, and the KU Leuven-University of Melbourne Joint Ph.D. Program.

References

[1] J. Sorocki and I. Piekarz, "Broadband dielectric spectroscopy of liquids using two-wire sensor towards their content analysis," in *2023 IEEE MTT-S International Microwave Biomedical Conference (IMBioC)*, 2023, pp. 139–141.

[2] Q. Xue, X. Tang, Y. Li, H. Liu, and X. Duan, "Contactless and simultaneous measurement of water and acid contaminations in oil using a flexible microstrip sensor," *ACS sensors*, vol. 5, no. 1, pp. 171–179, 2019.

[3] E. Porter *et al.*, "A wearable microwave antenna array for time-domain breast tumor screening," *IEEE Transactions on Medical Imaging*, vol. 35, no. 6, pp. 1501–1509, 2016.

[4] H. Zhang *et al.*, "Flexible and stretchable microwave electronics: Past, present, and future perspective," *Advanced Materials Technologies*, vol. 6, no. 1, p. 2000759, 2021.

[5] Q. Xue *et al.*, "Nanostrip flexible microwave enzymatic biosensor for noninvasive epidermal glucose sensing," *Nanoscale Horizons*, vol. 5, no. 6, pp. 934–943, 2020.

[6] A. Chahadih *et al.*, "Microwave/microfluidic sensor fabricated on a flexible kapton substrate for complex permittivity characterization of liquids," *Sensors and Actuators A: Physical*, vol. 229, pp. 128–135, 2015.

[7] A. Rahman, M. T. Islam, M. J. Singh, S. Kibria, and M. Akhtaruzzaman, "Electromagnetic performances analysis of an ultra-wideband and flexible material antenna in microwave breast imaging: To implement a wearable medical bra," *Scientific reports*, vol. 6, no. 1, p. 38906, 2016.

[8] K. Zhang, P. J. Soh, and S. Yan, "Design of a compact dual-band textile antenna based on metasurface," *IEEE Transactions on Biomedical Circuits and Systems*, vol. 16, no. 2, pp. 211–221, 2022.

[9] M. M. H. Mahfuz *et al.*, "Wearable textile patch antenna: Challenges and future directions," *IEEE Access*, vol. 10, pp. 38 406–38 427, 2022.

[10] B. Harkinezhad *et al.*, "Flexible microwave biosensor for liquid characterization inside laboratory containers," in *2023 IEEE MTT-S International Microwave Biomedical Conference (IMBioC)*, 2023, pp. 28–30.